Redox modulation of field-induced tetrathiafulvalene-based single-molecule magnets of dysprosium

S. Tiaouinine, J.F. Gonzalez, V. Montigaud, C.A. Mattei, V. Dorcet, L. Kaboub, V. Cherkasov, O. Cador, Boris Le Guennic, L. Ouahab, et al.

magnetochemistry

MDPI

Article

Redox Modulation of Field-Induced Tetrathiafulvalene-Based Single-Molecule Magnets of Dysprosium

Siham Tiaouinine [1,2], Jessica Flores Gonzalez [1], Vincent Montigaud [1], Carlo Andrea Mattei [1], Vincent Dorcet [1], Lakhmici Kaboub [1], Vladimir Cherkasov [3], Olivier Cador [1], Boris Le Guennic [1], Lahcène Ouahab [1], Viacheslav Kuropatov [3,*] and Fabrice Pointillart [1,*]

1 Univ Rennes, CNRS, ISCR (Institut des Sciences Chimiques de Rennes)—UMR 6226, F-35000 Rennes, France; sihamtiaouinine@yahoo.fr (S.T.); jessica.flores-gonzales@univ-rennes1.fr (J.F.G.); vincent.montigaud@univ-rennes1.fr (V.M.); carlo-andrea.mattei@univ-rennes1.fr (C.A.M.); vincent.dorcet@univ-rennes1.fr (V.D.); lkaboub@hotmail.com (L.K.); olivier.cador@univ-rennes1.fr (O.C.); boris.leguennic@univ-rennes1.fr (B.L.G.); lahcene.ouahab@univ-rennes1.fr (L.O.)

2 Laboratory of Organic Materials and Heterochemistry, University of Tebessa, Rue de Constantine, 12002 Tébessa, Algeria

3 G. A. Razuvaev Institute of Organometallic Chemistry of Russian Academy of Sciences, GSP-445, Tropinina str., 49, 603950 Nizhny Novgorod, Russia; cherkasov@iomc.ras.ru

* Correspondence: viach@iomc.ras.ru (V.K.); fabrice.pointillart@univ-rennes1.fr (F.P.)

Received: 8 July 2020; Accepted: 31 July 2020; Published: 19 August 2020

Abstract: The complexes $[Dy_2(tta)_6(\mathbf{H2SQ})]$ (**Dy-H_2SQ**) and $[Dy_2(tta)_6(\mathbf{Q})]\cdot 2CH_2Cl_2$ (**Dy-Q**) (tta^- = 2-thenoyltrifluoroacetonate) were obtained from the coordination reaction of the $Dy(tta)_3\cdot 2H_2O$ units with the 2,2′-benzene-1,4-diylbis(6-hydroxy-4,7-di-tert-butyl-1,3-benzodithiol-2-ylium-5-olate ligand (**H_2SQ**) and its oxidized form 2,2′-cyclohexa-2,5-diene-1,4-diylidenebis(4,7-di-tert-butyl-1,3-benzodithiole-5,6-dione (**Q**). The chemical oxidation of **H_2SQ** in **Q** induced an increase in the coordination number from 7 to 8 around the Dy^{III} ions and by consequence a modulation of the field-induced Single-Molecule Magnet behavior. Computational results rationalized the magnetic properties of each of the dinuclear complexes.

Keywords: Dysprosium; tetrathiafulvalene; Redox-Modulation; single molecule magnets; ab initio calculations

1. Introduction

One of the most promising routes of research in molecular magnetism is the design of lanthanide coordination complexes [1–4]. Such compounds are able to display magnetic bistability even for mononuclear species [5] due to the intrinsic characteristics of the lanthanide ions [6]. Recently, the observation of memory effects at temperatures close to liquid nitrogen [7–10] led to the revival of the use of such coordination systems for potential applications in high-density data storage [11,12]. Other applications could be targeted such as switches and sensors [13] when the magnetic properties can be modulated by chemical transformations. The modulations of Single-Molecule Magnet (SMM) behavior can be achieved via crystal-to-crystal chemical transformations [14–16], solvato-switching [17–19], isomerization-switching [20–24] or redox-switching [25–27]. Indeed, the magnetic properties of the lanthanide ions can be easily changed by structural transformation since they are very sensitive to the symmetry and electronic distribution of their surroundings [28]. The literature shows that structural changes can be induced by the use of redox active ligands [25–27]. Thus, the combination of

lanthanide ions and redox-active ligands seems to be a right way to design SMM with modulations of the magnetic behavior.

In the past, some of us already explored this strategy to design redox-active (chiral) SMMs [29,30] and luminescent SMMs [31]. On one hand, the 4,4′,7,7′-tetra-tert-butyl-2,2′-bi-1,3-benzodithiole-5,5′,6,6′-tetrone [32] and 2,2′-benzene-1,4-diylbis(6-hydroxy-4,7-di-tert-butyl-1,3-benzodithiol-2-ylium-5-olate [33] ligands (**H_2SQ**) (Scheme 1) were used to bridge magnetic lanthanide units [34,35]. On the other hand, the **H_2SQ** ligand and its oxidized form 2,2′-cyclohexa-2,5-diene-1,4-diylidenebis(4,7-di-tert-butyl-1,3-benzodithiole-5,6-dione (**Q**) (Scheme 1) were associated with Ln(hfac)$_3$ units (Ln = Dy^{III} [36] and Yb^{III} [37]) for modulating both magnetic and photo-physical properties.

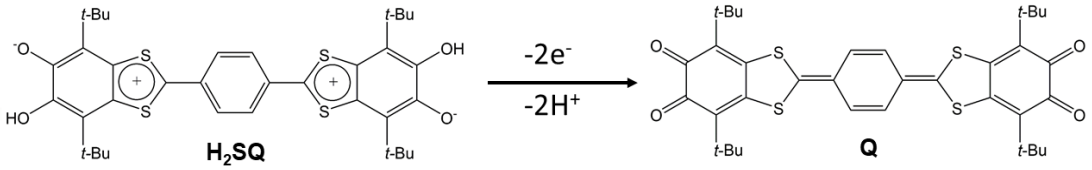

Scheme 1. Oxidation reaction of the **H_2SQ** ligand in **Q** ligand with their molecular structures.

In the present article, we propose to focus our attention on the **H_2SQ** ligand and its oxidized form **Q** in the coordination reactions with the Dy(tta)$_3$·2H_2O units. The replacement of the $hfac^-$ ancillary anions with tta^- is known to change the magnetic performances of the target compound [29,38–40]. Indeed, the resulting X-ray structures of the dinuclear complexes [Dy_2(tta)$_6$(**H_2SQ**)] (**Dy-H_2SQ**) and [Dy_2(tta)$_6$(**Q**)]·2CH_2Cl_2 (**Dy-Q**) highlighted new coordination spheres around the Dy^{III} compared to those observed for their $hfac^-$ parents of formula [Dy_2(hfac)$_6$(**H_2SQ**)]·CH_2Cl_2 and [Dy_2(hfac)$_6$(**Q**)]) [36] leading to the study of new magnetic properties. Then the modulation of the magnetic properties as consequence of the oxidation of the bridging triads was evaluated.

2. Results and Discussion

2.1. X-ray Structures

The coordination reaction of the 2,2′-benzene-1,4-diylbis(6-hydroxy-4,7-di-tert-butyl-1,3-benzodithiol-2-ylium-5-olate triad (**H_2SQ**) (Scheme 1) and tris(2-thenoyltrifluoroacetonate)bis(aqueous)Ln^{III} (Dy(tta)$_3$·2H_2O) in CH_2Cl_2 led to the formation of the complex [Dy_2(tta)$_6$(**H_2SQ**)] (**Dy-H_2SQ**). Prior oxidation of **H_2SQ** into **Q** using an excess of MnO_2, followed by coordination reaction with Dy(tta)$_3$·2H_2O led to the [Dy_2(tta)$_6$(**Q**)]·2CH_2Cl_2 (**Dy-Q**) complex.

[Dy_2(tta)$_6$(**H_2SQ**)] (**Dy-H_2SQ**). **Dy-H_2SQ** crystallized in the monoclinic space group C2/c (Figure 1 and Figure S1, Table S1). The asymmetric unit is composed by one half of the [Dy_2(tta)$_6$(**H_2SQ**)] dinuclear specie. Each of the two terminal coordination sites are occupied by one Ln(tta)$_3$ unit. The coordination takes place through the C-O^- group while the C-OH group remains free. Such mono-chelating coordination mode was already observed in the formation of the 1D compound {[Dy(hfac)$_3$(**H_2SQ**)]·2C_6H_{14}}$_n$ [35]. The confirmation of the bis mono-protonated form of the triad is given by the specific C-O7 (1.316 Å) and C-O8 (1.347 Å) distances as well as the torsion angle of 30.3(2)° between the 6-hydroxy-4,7-di-tert-butyl-1,3-benzodithiol and *p*-phenylene moieties that have previously been observed for the free ligand [33]. The non-planarity of the triad is an indication of a possible charge-separated structure (Scheme 1) instead of a bis radical semiquinone structure because it is possible only if the C39-C40 bond has a single character as observed (1.484 Å) in the experimental X-ray structure of **Dy-H_2SQ** compound. The X-ray structure further confirmed the charge-separated structure. Indeed, the 1,3-dithiole rings are close to being aromatic since the S1-C39 (1.691(9) Å) and S2-C39 (1.667(8) Å) are similar with those for tetrathiafulvanene (TTF) dications (1.670–1.690 Å). In comparison, such chemical bonds are longer in neutral TTF (1.730–1.760 Å) [41–43]. The typical

o-quinone bond lengths are different compared to those in the terminal six-membered rings in bridging ligand in **Dy-H_2SQ**. Thus, each Dy^{III} ion is surrounded by seven oxygen atoms coming from the three tta^- anions and the monochelating **H_2SQ** ligand, which is a quite unusual coordination polyhedron for trivalent lanthanide. The increase in steric hindrance replacing the $hfac^-$ anions with tta^- ones led to an unusual decrease in the coordination number from 8 to 7.

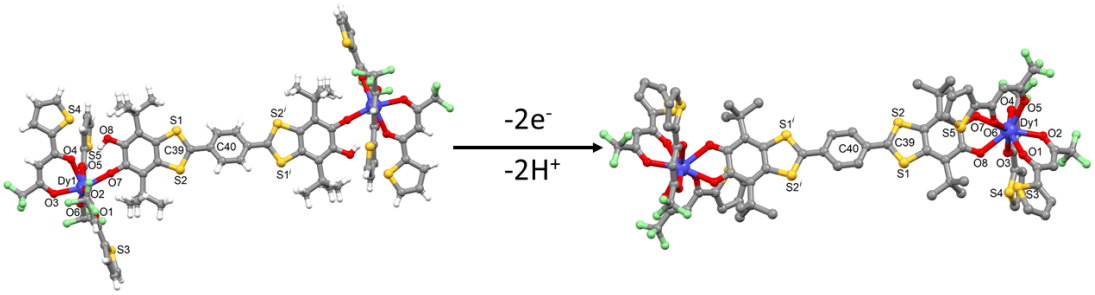

Figure 1. Molecular structures of **Dy-H_2SQ** (**on the left**) and its oxidized form **Dy-Q** (**on the right**). Hydrogen atoms and molecules of crystallization are omitted for clarity.

The average Dy-O bond length is 2.295 Å but there is a significant difference between the Dy-O_{tta} (2.309 Å) and Dy-O7 (2.208 Å) distances.

The crystal packing reveals the formation of an organic sub-network of **H_2SQ** triads along the *c* axis (Figure 2). The stabilization of such a sub-network is possible thanks to π–π interactions between the 1,3-benzodithiol and S2···S4 contacts (3.788 Å) between the 1,3-benzodithiol and tta^- anions (Figure 2). The Dy–Dy intramolecular distance is 22.233 Å while the shortest Dy–Dy intermolecular distance is 10.217 Å.

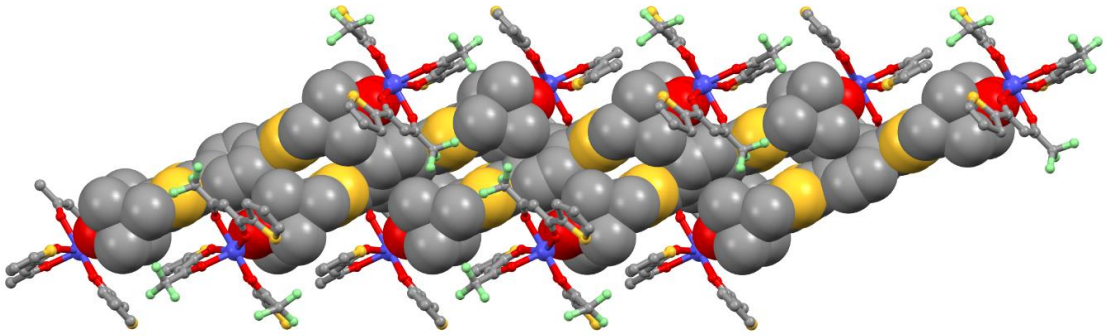

Figure 2. Crystal packing of **Dy-H_2SQ** along the c axis. "Spacefill" and "ball and sticks" representations are used for **H_2SQ** ligands and $Dy(tta)_3$ units, respectively.

$[Dy_2(tta)_6(\mathbf{Q})]\cdot 2CH_2Cl_2$ (**Dy-Q**). **Dy-Q** crystallized in the monoclinic space group $P2_1/c$ (Figure 1 and Figure S2, Table S1). The asymmetric unit is composed by one half of the $[Dy_2(tta)_6(\mathbf{Q})]$ dinuclear species and one dichloromethane molecule of crystallization. The two quinone coordination sites are occupied by a $Ln(tta)_3$ unit with a bischelating mode. The oxidation of the triad in **Q** is confirmed by the double character of the C=O7 (1.246 Å) and C=O8 (1.243 Å) chemical bonds, which are shorter than the ones in the **H_2SQ** triad. It is also worth noting the decreasing of the torsion angle (9.4(1)°) between the central six-membered ring and bicyclic planes because of the increasing of the aromaticity character of the ligand after oxidation. It was established previously that such an oxidized form cannot be isolated in solid-state due to its instability [33]. Thus, one could conclude that the coordination of both electron withdrawing $Dy(tta)_3$ units led to an energy stabilization of the **Q** triad. The two Dy^{III} ions are surrounded by eight oxygen atoms coming from the three tta^- anions and the bischelating **Q** ligand. The average Dy-O_{tta} and Dy-O_Q are, respectively, equal to 2.327 Å and 2.413 Å, making the average Dy-O bond length (2.349 Å) longer than for **Dy-H_2SQ**. Such observations can be explained

by two reasons: (i) the difference of electronic effect between **H_2SQ** vs. **Q** i.e., the charge carried by the coordination sites of **H_2SQ** is more negative than those for **Q** and (ii) the seven-coordination in **Dy-H_2SQ** vs. eight-coordination in **Dy-Q**. Once more, the replacement of $hfac^-$ with tta^- anions decreased the coordination number from 9 to 8.

Consequently, the oxidation of the triad led to drastic changes in the coordination number and symmetry of the lanthanide surroundings and one could anticipate different magnetic behaviors between the two **Dy-H_2SQ** and **Dy-Q** dinuclear complexes.

The crystal packing of **Dy-Q** is depicted in Figure 3. It highlighted isolated **Q** triads and stacking of the dinuclear complexes through π–π interactions and S2···S3 (3.991 Å) between the extended TTF and two tta^- anions. Similar organization of the molecules was found in the crystal packing when the 4,4′,7,7′-tetra-tert-butyl-2,2′-bi-1,3-benzo-dithiole-5,5′,6,6′-tetrone triad was used instead of **Q** [34]. The Dy–Dy intramolecular distance is 21.729 Å while the shortest Dy–Dy intermolecular distance is 10.099 Å.

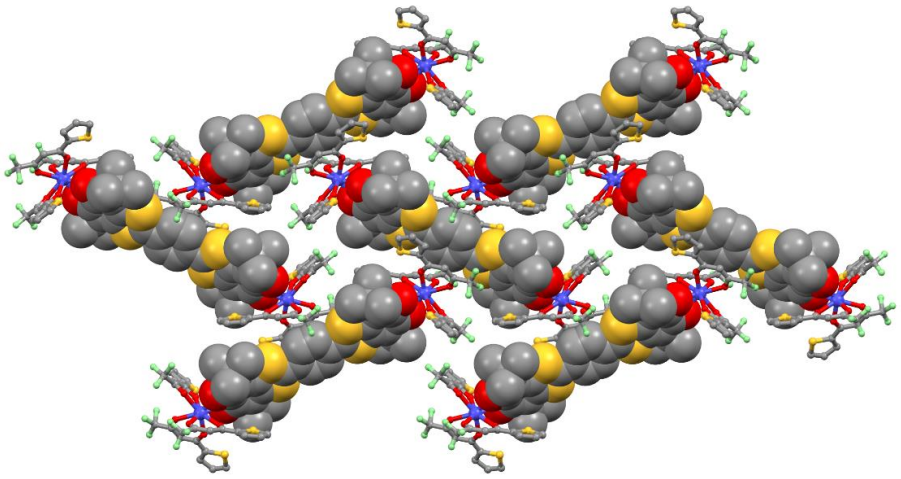

Figure 3. Crystal packing of **Dy-Q**. "Spacefill" and "ball and sticks" representations are used for **Q** ligands and $Dy(tta)_3$ units, respectively.

2.2. Magnetic Properties

2.2.1. Static Magnetic Measurements

The dc magnetic properties of **Dy-H_2SQ** and **Dy-Q** were studied measuring the temperature dependence of the magnetic susceptibility. The ${}_MT(T)$ curves are depicted in Figure 4.

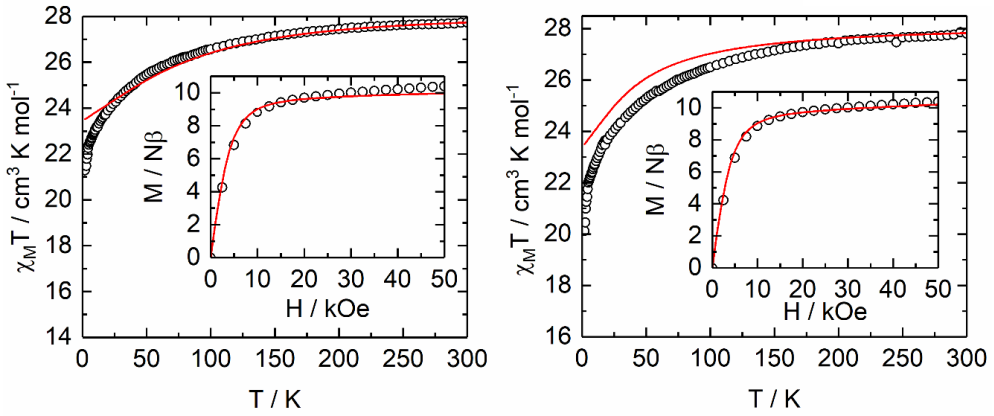

Figure 4. (**left**) Temperature dependence of $\chi_M T$ for **Dy-H_2SQ** and (**right**) **Dy-Q**. Inset, the field variations of the magnetization at 2 K for **Dy-H_2SQ** (**left**) and **Dy-Q** (**right**). The ab initio simulated curves are represented in red.

The 27.73 $cm^3 \cdot K \cdot mol^{-1}$ and 27.81 $cm^3 \cdot K \cdot mol^{-1}$ room temperature values for **Dy-H_2SQ** and **Dy-Q** compounds are close to the expected value considering two isolated Dy^{III} ions ($^6H_{15/2}$ ground state multiplet) (28.34 $cm^3 \cdot K \cdot mol^{-1}$) [44]. $_MT$ products decrease monotonically down to 20.82 $cm^3 \cdot K \cdot mol^{-1}$ for **Dy-H_2SQ** and 20.12 $cm^3 \cdot K \cdot mol^{-1}$ for **Dy-Q** when decreasing the temperature. Such behavior is attributed to the thermal depopulation of the M_J states. The expected saturated value of 20 μB for the field dependence of the magnetization measured at 2.0 K for both dinuclear compounds are not reached since at 50 kOe, **Dy-H_2SQ** and **Dy-Q** exhibited respective experimental values of 10.03 μB and 10.40 μB, highlighting the magnetic anisotropy of the systems [44].

2.2.2. Dynamic Magnetic Measurements

The dynamic magnetic properties were studied, measuring the molar ac magnetic susceptibility (χ_M) for both compounds **Dy-H_2SQ** and **Dy-Q**. An out-of-phase signal (χ_M″) was detected at high frequency in zero magnetic field but the maxima are localized out of the frequency range 1–1000 Hz for both **Dy-Q** and **Dy-H_2SQ** (Figure 5a, Figures S3 and S4).

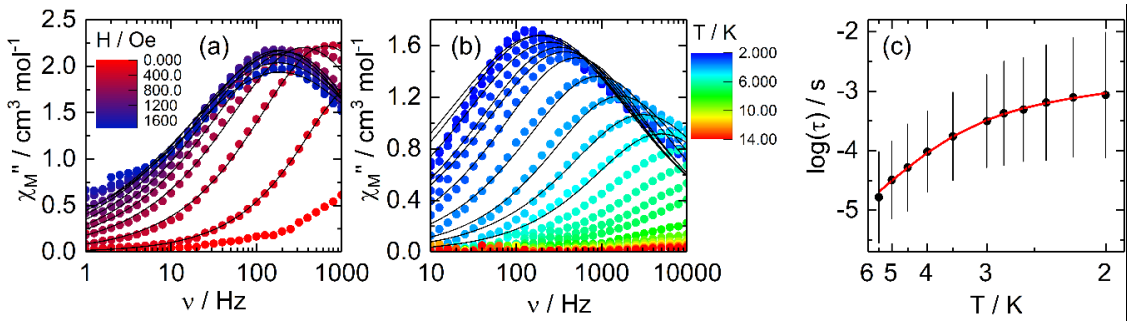

Figure 5. (**a**) Frequency dependence of χ_M″ between 0 and 1800 Oe for **Dy-Q** at 2 K with the best fitted curves, (**b**) Frequency dependence of χ_M″ between 2 and 15 K for **Dy-Q** at 1200 Oe with the best fitted curves and (**c**) temperature variation of the relaxation time for **Dy-Q** in the temperature range of 2–5.5 K with the best fitted curve with the modified Arrhenius law (red line). Error lines are calculated using the log-normal distribution model at the 1 σ level [45].

The most common reason for the fast magnetic relaxation is the existence of quantum tunneling of the magnetization (QTM). The application of a magnetic dc field is a well-known method to cancel the QTM. The magnetic susceptibility was then measured under various applied magnetic fields (Figure 5a, Figures S3 and S4). For both compounds, the application of a small magnetic field led to a shift of the out-of-phase component of the magnetic susceptibility within the experimental windows and the magnetic field value of 1200 Oe was chosen as a good compromise between relaxation time and intensity for **Dy-H_2SQ** (Figure S4) and the optimal magnetic field for **Dy-Q** (Figure 5a) as highlighted by the field dependence of the log(τ) (Figures S5 and S6). Under such an applied field, **Dy-H_2SQ** highlighted a frequency dependence of the out-of-phase signal of the susceptibility (Figures S7 and S8). Unfortunately the χ''_M signal is very broad, ranging from 100 to 10,000 Hz between 2 and 15 K, and extraction of the relaxation times for this compound using the extended Debye model failed. Under the same applied field of 1200 Oe, **Dy-Q** highlighted a frequency dependence of the magnetic susceptibility (Figure 5b and Figure S7), which can be analyzed in the framework of the extended Debye model [46,47]. The extended Debye model was applied to fit simultaneously the experimental variations of χ_M′ and χ_M″ with the frequency ν of the oscillating field ($\omega = 2\pi\nu$) (Figure S9). The temperature dependence of the relaxation time is extracted and depicted in Figure 5c (Table S2). A large fraction of the sample shows slow relaxation of the magnetization as depicted by the

normalized Argand (Figure S10). The relaxation time of the magnetization (τ) follows two thermally dependent processes of relaxation:

$$\tau^{-1} = \underbrace{CT^n}_{Raman} + \underbrace{\tau_0^{-1} \exp\left(-\frac{\Delta}{KT}\right)}_{Orbach}$$

The best fit was obtained with $\tau_0 = 1.9(7) \times 10^{-7}$ s and $\Delta = 18.4(2)$ cm^{-1}, and C = 289(93) s^{-1}K^{-n} and $n = 1.88(39)$ (Figure 5c). The expected n value for Kramers ions should be 9 [48] but the presence of both acoustic and optical phonons could lead to lower values between 2 and 7 [49–51] or even lower for the crystalline phase of Dy^{III} coordination complexes [7–10,52].

As expected from the drastic structural changes for the Dy^{III} coordination spheres after oxidation of the bridging ligand, the dynamic magnetic behaviors are also strongly affected. In fact the out-of-phase signal became narrower and the maximum of the χ_M" at 2 K was shifted from 1000 Hz to 125 Hz after oxidation. In other words, the oxidation of the bridging triad led to an enhancement of the SMM performances. It is worth noting that a reverse trend was observed for the parent compounds based on the $Dy(hfac)_3$ units [36]. For the latter analogues, the strong degradation of the magnetic performances after oxidation of the bridging triad was imputed to both change of coordination number from 8 to 9 and the strong variation of intermolecular dipolar magnetic interaction because of the presence of hydrogen bond in the oxidized compound leading to a shortening of the intermolecular Dy–Dy distance from 9.962 Å to 6.071 Å. For **Dy-H_2SQ** and **Dy-Q**, the role of the intermolecular dipolar interactions cannot be put aside but their change of intensity are expected to be much weaker than for their $Dy(hfac)_3$ based-parents since the intermolecular Dy–Dy distances remain very long (10.217 Å and 10.099 Å). In terms of magnetic performances, the following trend was observed at 2 K under an applied field of 1200 Oe: **Dy-H_2SQ** (1000 Hz) < **Dy-Q** (125 Hz) < $[Dy_2(hfac)_6(H_2O)_2(\mathbf{Q})]$ (25 Hz) < $[Dy_2(hfac)_6(\mathbf{H_2SQ})]\cdot CH_2Cl_2$ (0.04 Hz). One could conclude that the $Dy(hfac)_3$ analogues displayed better dynamic magnetic properties than the compounds involving the $Dy(tta)_3$ units and the magnetic modulation is more efficient for $[Dy_2(hfac)_6(\mathbf{H_2SQ})]\cdot CH_2Cl_2$ and $[Dy_2(hfac)_6(H_2O)_2(\mathbf{Q})]$ than for **Dy-H_2SQ** and **Dy-Q**.

2.2.3. Ab Initio Calculations

State-Averaged Complete Active Space Self-Consistent Field approach with restricted-active-space-state-interaction method (SA-CASSCF/RASSI-SO) calculations were carried out for the two dinuclear complexes **Dy-H_2SQ** and **Dy-Q** to rationalize the observed magnetic properties. Since the two dinuclear complexes are centrosymmetric, only half of the complex, i.e., one metal center, was taken into account. The experimental χ_MT vs. T and M vs. H curves (Figure 4) are fairly well reproduced by the ab initio calculations. The inconsistence between experimental χ_MT product and calculations at low temperature could be due to the presence of antiferromagnetic dipolar interaction, which has not been taken into account in the calculations. The Dy ion in **Dy-H_2SQ** presents a strongly mixed ground state (34% M_J = | ± 13/2>, 25% M_J = | ± 15/2>, 15% M_J = | ± 11/2> and 10% M_J = | ± 7/2>, Table S3) defined by a g-tensor with a main component $g_Z = 15.08$ and exhibiting non-negligible transversal components with $g_X = 0.11$, $g_Y = 1.10$ confirming the low anisotropy character of the ground state (for a pure M_J = | ± 15/2 > ground state, the fully axial, Ising-type, g-tensor expected possess $g_X = g_Y = 0.0$ and $g_Z = 20.0$) and the presence of efficient QTM at zero-applied magnetic field. After oxidation of the **H_2SQ** triad in the **Q** one, the change of the seven-coordination sphere into the eight-coordination sphere around the Dy^{III} center induced drastic changes in the electronic properties since an almost Ising ground state was now calculated for the Dy in **Dy-Q** (90% M_J = | ± 15/2>, Table S4). The transversal components of the magnetic anisotropy tensor are still present ($g_X = 0.05$, $g_Y = 0.11$), justifying the existence of QTM, but they are much weaker than those for **Dy-H_2SQ**. At this point,

the difference of relaxation time below 4 K can be explained by the difference of magnetic anisotropy generated by the seven and eight coordination sphere.

The main component of the ground state g-tensor of the Dy^{III} centers for each complex is represented in Figure 6. For both systems, the main magnetic component appears perpendicular to the plane containing the reduced protonated form of the coordinating moiety (for **Dy-H_2SQ**, left part of the Figure 6) and the quinone moiety (for **Dy-Q**, right part of the Figure 6) i.e., the most charged direction as expected for an oblate ion [4].

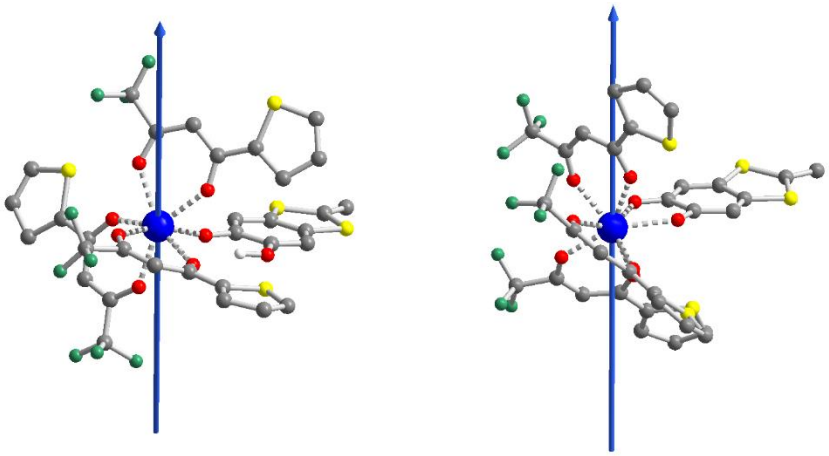

Figure 6. Orientations of the ground state g-tensor main component (g_Z) characterizing the magnetic anisotropy calculated on each Dy^{III} center (blue vectors) for the molecular structures of **Dy-H_2SQ** (**left**) and **Dy-Q** (**right**).

The transversal magnetic moments between the M_J levels for the Kramers ions of each complex have been computed in order to give more insights into the relaxation mechanisms (Figure 7). A major difference between the two compounds is the large quantum-tunneling elements (0.20 μB and 0.26 μB for the ground and first excited states, respectively) for **Dy-H_2SQ** while **Dy-Q** displays much weaker QTM values. These differences, which are directly related with the transversal components of the anisotropy tensors, are in the trend of the experimental results with a faster relaxation of the magnetization for **Dy-H_2SQ** than for **Dy-Q**. The difference between the calculated energy barrier (Δ = 80 cm^{-1}) and the experimental barrier (Δ = 18.4 cm^{-1}) can be explained by operating an under-barrier relaxation mechanism such as the Raman process [53–56].

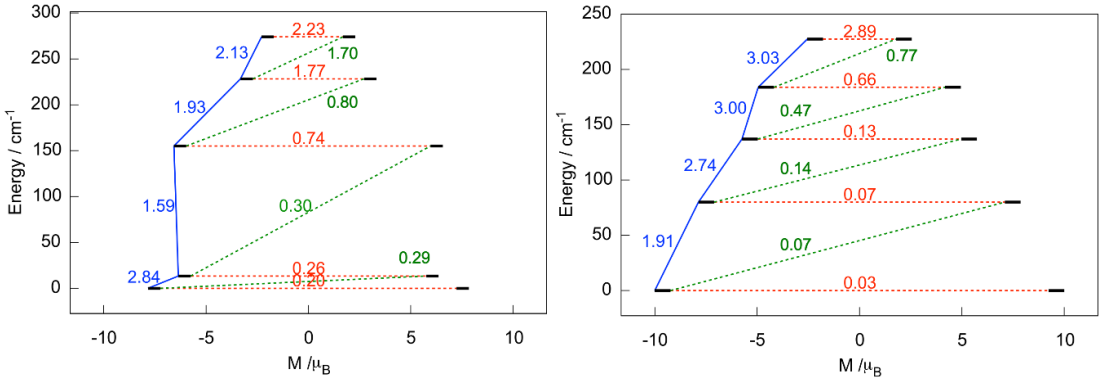

Figure 7. Computed magnetization blocking barrier in complexes **Dy-H_2SQ** (**left**) and **Dy-Q** (**right**). Numbers provided on each arrow are the mean absolute values for the corresponding matrix elements of the magnetic transition dipole moment.

3. Materials and Methods

3.1. Synthesis General Procedures and Materials

The precursor $Dy(tta)_3{\cdot}2H_2O$ (tta^- = 2-thenoyltrifluoroacetonate anion) [57] and the 2,2′-benzene-1,4-diylbis(6-hydroxy-4,7-di-tert-butyl-1,3-benzodithiol-2-ylium-5-olate ligand [33] (**H_2SQ**) were synthesized following previously reported methods. All other reagents were commercially available and used without further purification.

3.2. Synthesis of complexes $[Dy_2(tta)_6(H_2SQ)]$ (DySQ) (Dy-H_2SQ) and $[Dy_2(tta)_6(Q)]{\cdot}2CH_2Cl_2$ (Dy-Q)

$[Dy_2(tta)_6$(**H_2SQ**)] (**Dy-H_2SQ**). 68.8 mg of $Dy(tta)_3{\cdot}2H_2O$ (0.08 mmol) were dissolved in 10 mL of CH_2Cl_2 and then added to a purple solution of 10 mL of CH_2Cl_2 containing 26.4 mg of **H_2SQ** (0.04 mmol). The solution of **H_2SQ** changed color from purple to blue, adding the Dy^{III} salt. After 15 min of stirring, 20 mL of *n*-hexane were layered at room temperature. Slow diffusion in the dark leads to deep blue single crystals of **DyH$_2$SQ**, which are suitable for X-ray diffraction experiments. Yield (determined from isolated single crystals) 56.6 mg (61%). Anal. Calcd (%) for $C_{84}H_{66}Dy_2F_{18}O_{16}S_{10}$: C 43.47, H 2.85; found: C 43.09, H 2.93.

$[Dy_2(tta)_6$(**Q**)]·$2CH_2Cl_2$ (**Dy-Q**). 13.2 mg of **H_2SQ** (0.02 mmol) were dissolved in 20 mL of CH_2Cl_2 and then stirred in the presence of 1.5 g of MnO_2. The starting purple solution turned green (oxidation of **H_2SQ** into **Q**) and after 45 min of stirring it was filtered directly in a CH_2Cl_2 solution (5 mL) of $Dy(tta)_3{\cdot}2H_2O$ (34.4 mg, 0.04 mmol). The green solution turned to a dark pink color. Slow diffusion of *n*-hexane into the resulting dark pink solution led to the formation of single crystals of **Dy-Q**, which are suitable for X-ray diffraction experiments. Yield (determined from isolated single crystals) 19.4 mg (39%). Anal. Calcd (%) for $C_{86}H_{68}Dy_2F_{18}Cl_4O_{16}$: C 41.50, H 2.73; found: C 42.07, H 2.79.

3.3. Crystallography

Single crystals of **Dy-H_2SQ** and **Dy-Q** were mounted on a APEXIII D8 VENTURE Bruker-AXS diffractometer for data collection (MoK_α radiation source, λ = 0.71073 Å), from the Diffractometric center (CDIFX), University of Rennes 1, France (Table S1). Structures were solved with a direct method using the SHELXT program [58] and refined with a full matrix least-squares method on F^2 using the SHELXL-14/7 program [59]. The SQUEEZE procedure of PLATON [60] was performed for **Dy-H_2SQ** because it contains large solvent accessible voids in which residual peaks of diffraction were observed. The CCDC number is 1898867 and 1898866 for compounds **Dy-H_2SQ** and **Dy-Q**, respectively.

3.4. Physical Measurements

The elemental analyses of the compounds were performed at the Centre Régional de Mesures Physiques de l'Ouest, Rennes. The static susceptibility measurements were performed on solid polycrystalline samples with a Quantum Design MPMS-XL SQUID magnetometer. Magnetic field values of 0.2 kOe, 2 kOe and 10 kOe were, respectively, applied for the temperature range of 2–20 K, 20–80 K and 80–300 K. These measurements were realized from immobilized selected and crunched single crystals and they were all corrected for the diamagnetic contribution, as calculated with Pascal's constants. The ac magnetic susceptibility measurements were performed on both a Quantum Design MPMS-XL SQUID magnetometer (1–1000 Hz frequency range) and a Quantum Design PPMS (10–10,000 Hz frequency range) system equipped with an ac/dc probe.

3.5. Computational Details

The atomic positions were extracted from the X-ray diffraction crystal structures of the **Dy-H_2SQ** and **Dy-Q** compounds. The two Dy^{III} magnetic centers were equally treated since the dinuclear complexes are centrosymmetric.

The State-Averaged Complete Active Space Self-Consistent Field approach with the restricted-active-space-state-interaction method (SA-CASSCF/RASSI-SO), as implemented in the MOLCAS quantum-chemistry package (version 8.0), was used to perform all ab-initio calculations [61]. The relativistic effects were treated in two steps on the basis of the Douglas–Kroll Hamiltonian. The CASSCF wavefunctions and energies were determined from the inclusion of the scalar terms in the basis-set generation [62]. Spin–orbit coupling was then added within the RASSI-SO method, which mixes the calculated CASSCF wavefunctions [63,64]. The resulting spin–orbit wavefunctions and energies were used to compute the magnetic properties and g-tensors of the ground state multiplet following the pseudospin S = 1/2 formalism, as implemented in the SINGLE-ANISO routine [55,65]. In order to save disk space and to accelerate the calculations, Cholesky decomposition of the bielectronic integrals was employed [66].

The active space considered in the calculations consisted of the nine 4f electrons of the Dy(III) ion, spanning the seven 4f orbitals; that is, CAS(9,7)SCF. State-averaged CASSCF calculations were performed for all of the sextets (21 roots), all of the quadruplets (224 roots) and 300 out of the 490 doublets of the Dy^{III} ion. Twenty-one sextets, 128 quadruplets and 107 doublets were mixed through spin–orbit coupling in RASSI-SO. All atoms were described with ANO-RCC basis sets with the following contractions [8s7p4d3f2g1h] for Dy; [7s6p4d2f] for Y; [4s3p2d] for the O and N atoms; [3s2p1d] for C of the first coordination sphere and [3s2p] for the other C atoms; [2s1p] for F; [4s3p1d] for S atoms and [2s] for the H atoms [67,68].

4. Conclusions

In this article, the 2,2′-benzene-1,4-diylbis(6-hydroxy-4,7-di-tert-butyl-1,3-benzodithiol-2-ylium-5-olate triad (**H_2SQ**) allowed the bridging of two $Dy(tta)_3$ units leading to the formation of the dinuclear complex of formula $[Dy_2(tta)_6(\mathbf{H_2SQ})]$ (**Dy-H_2SQ**). After the chemical oxidation of the **H_2SQ** triad, the resulting 2,2′-cyclohexa-2,5-diene-1,4-diylidenebis(4,7-di-tert-butyl-1,3-benzodithiole-5,6-dione **Q** triad allowed the formation of the new dinuclear $[Dy_2(tta)_6(\mathbf{Q})]\cdot 2CH_2Cl_2$ complex (**Dy-Q**). The oxidation of the triad induced changes of the coordination number from seven to eight and thus the coordination polyhedron symmetry is modified. Both compounds behave as field-induced SMM with a slowing down of the magnetic relaxation after oxidation. Wavefunction calculations showed that the change from coordination number seven to eight induced an increase in the Ising character of the magnetic anisotropy.

Supplementary Materials: The following are available online at http://www.mdpi.com/2312-7481/6/3/34/s1, Figure S1. ORTEP view of **Dy-H_2SQ**. Thermal ellipsoids are drawn at 30% probability. Hydrogen atoms are omitted for clarity; Figure S2. ORTEP view of **Dy-Q**. Thermal ellipsoids are drawn at 30% probability. Hydrogen atoms and solvent molecules of crystallization are omitted for clarity; Figure S3. (left) Frequency dependence of χ_M' between 0 and 3000 Oe for **Dy-H_2SQ** at 2 K, (b) Frequency dependence of χ_M' between 0 and 1600 Oe for **Dy-Q** at 2 K.; Figure S4. Frequency dependence of χ_M'' between 0 and 3000 Oe for **Dy-H_2SQ** at 2K; Figure S5. Representation of the field-dependence of the relaxation time of the magnetization for **Dy-H_2SQ** at 2 K.; Figure S6. Representation of the field-dependence of the relaxation time of the magnetization for **Dy-Q** at 2 K.; Figure S7. Frequency dependence of χ_M' between 2 and 15 K at 1200 Oe for **Dy-H_2SQ** (left) and **Dy-Q** (right); Figure S8. Frequency dependence of χ_M'' between 2 and 15 K for **Dy-H_2SQ** at 1200 Oe; Figure S9. Frequency dependence of the in-phase (χ_M') and out-of-phase (χ_M'') components of the ac susceptibility measured on powder at 4 K and 1200 Oe with the best fitted curves (red lines) for **Dy-Q**; Figure S10. Normalized Argand plot for **Dy-Q** between 2 and 5 K; Figure S8. Frequency dependence of the in-phase (χ_M') and out-of-phase (χ_M'') components of the ac susceptibility measured on powder at 4 K and 1200 Oe with the best fitted curves (red lines) for **Dy-Q**. Table S1: X-ray crystallographic data of **Dy-H_2SQ** and **Dy-Q**; Table S2: Best fitted parameters (χ_T, χ_S, τ and α) with the extended Debye model **Dy-Q** at 1200 Oe in the temperature range 2–5.5 K; Table S3: Computed energies, *g*-tensor and wavefunction composition of the ground state doublets in the effective spin $\frac{1}{2}$ model for **Dy-H_2SQ**; Table S4: Computed energies, *g*-tensor and wavefunction composition of the ground state doublets in the effective spin $\frac{1}{2}$ model for **Dy-Q**.

Author Contributions: V.C. and V.K. performed the organic syntheses; S.T. and C.A.M. and F.P. performed the coordination chemistry and crystallizations, V.D. realized the single crystal X-ray diffraction experiments and refined the X-ray structures; O.C. and J.F.G. performed and analyzed the magnetic measurements, V.M. and B.L.G. performed the ab initio calculations. L.O. and L.K. discussed the idea and the results and commented on the manuscript. F.P., V.K., O.C. and B.L.G. conceived and designed the experiments and contributed to the writing of the article. All authors have read and agreed to the published version of the manuscript.

Funding: This work was supported by CNRS, Université de Rennes 1, France-Russia MULTISWITCH PRC Grant (N°227606), Russian Federal Program (RFMEFI62120X0040) and the European Commission through the ERC-CoG 725184 MULTIPROSMM (project n. 725184).

Acknowledgments: B.L.G. and V.M. thank the French GENCI/IDRIS-CINES center for high-performance computing resources. V.K. and V.C. thank the "Analytical Center IOMC RAS". S.T. and L.K. thank the Algerian PNE program for the financial support during the stay in the French ISCR laboratory.

Conflicts of Interest: The authors declare no conflict of interest. The founding sponsors had no role in the design of the study; in the collection, analyses, or interpretation of data; in the writing of the manuscript, and in the decision to publish the results.

Abbreviations

The following abbreviations are used in this manuscript:

SMM	Single Molecule Magnet
QTM	Quantum Tunneling of the Magnetization
CH_2Cl_2	dichloromethane
tta-	2-thenoyltrifluoroacetonate
TTF	tetrathiafulvalene
CASSCF	Complete Active Space Self-Consistent Field
RASSI-SO	Restricted Active Space State Interaction—Spin–Orbit

References

1. Woodruff, D.N.; Winpenny, R.E.P.; Layfield, R.A. Lanthanide Single-Molecule Magnets. *Chem. Rev.* **2013**, *113*, 5110–5148. [CrossRef] [PubMed]
2. Sessoli, R.; Powell, A.K. Strategies towards single molecule magnets based on lanthanide ions. *Coord. Chem. Rev.* **2009**, *253*, 2328–2341. [CrossRef]
3. Pointillart, F.; Cador, O.; Le Guennic, B.; Ouahab, L. Uncommon Lanthanide ions in purely 4f Single Molecule Magnets. *Coord. Chem. Rev.* **2017**, *346*, 150–175. [CrossRef]
4. Rinehart, J.D.; Long, J.R. Exploiting single-ion anisotropy in the design of f-element single-molecule magnets. *Chem. Sci.* **2011**, *2*, 2078–2085. [CrossRef]
5. Ishikawa, N.; Sugita, M.; Ishikawa, T.; Koshihara, S.; Kaizu, Y. Lanthanide Double-Decker Complexes Functioning as Magnets at the Single-Molecular Level. *J. Am. Chem. Soc.* **2003**, *125*, 8694–8695. [CrossRef]
6. Carlin, R.L. *Magnetochemistry*; Springer: Berlin, Germany, 1986.
7. Guo, F.-S.; Day, B.-M.; Chen, Y.-C.; Tong, M.-L.; Mansikkamäki, A.; Layfield, R.A. A Dysprosium Metallocene Single-Molecule Magnet Functioning at the Axial Limit. *Angew. Chem.* **2017**, *56*, 11445–11449. [CrossRef]
8. Goodwin, C.A.P.; Ortu, F.; Reta, D.; Chilton, N.F.; Mills, D.P. Molecular magnetic hysteresis at 60 kelvin in dysprosocenium. *Nature* **2017**, *548*, 439–442. [CrossRef]
9. McClain, K.R.; Gould, C.A.; Chakarawet, K.; Teat, S.J.; Groshens, T.J.; Long, J.R.; Harvey, B.G. High-temperature magnetic blocking and magneto-structural correlations in a series of Dysprosium(III) metallocenium single-molecule magnets. *Chem. Sci.* **2018**, *9*, 8492–8503. [CrossRef]
10. Guo, F.-S.; Day, B.-M.; Chen, Y.-C.; Tong, M.-L.; Mansikkamäki, A.; Layfield, R.A. Magnetic hysteresis up to 80 kelvin in a Dysprosium metallocene single-molecule magnet. *Science* **2018**, *362*, 1400–1403. [CrossRef]
11. Mannini, M.; Pineider, F.; Sainctavit, P.; Danieli, C.; Otero, E.; Sciancalepore, C.; Talarico, A.M.; Arrio, M.-A.; Cornia, A.; Gatteschi, D.; et al. Magnetic memory of a single-molecule quantum magnet wired to a gold surface. *Nat. Mater.* **2009**, *8*, 194–197. [CrossRef]
12. Affronte, M. Molecular nanomagnets for information technologies. *J. Mater. Chem.* **2009**, *19*, 1731–1737. [CrossRef]
13. Sato, O. Dynamic molecular crystals with switchable physical properties. *Nat. Chem.* **2016**, *8*, 644–656. [CrossRef] [PubMed]
14. Wu, D.-Q.; Shao, D.; Wei, X.-Q.; Shen, F.-X.; Shi, L.; Kempe, D.; Zhang, Y.-Z.; Dunbar, K.R.; Wang, X.-Y. Reversible On-Off Switching of a Single-Molecule Magnet via a Crystal-to-Crystal Chemical Transformation. *J. Am. Chem. Soc.* **2017**, *139*, 11714–11717. [CrossRef] [PubMed]

15. Shao, D.; Shi, L.; Yin, L.; Wang, B.-L.; Wang, Z.-X.; Zhang, Y.-Q.; Wang, X.-Y. Reversible on-off switching of both spin crossover and single-molecule magnet behaviours via a crystal-to-crystal transformation. *Chem. Sci.* **2018**, *9*, 7986–7991. [CrossRef] [PubMed]
16. Zhang, X.; Vieru, V.; Feng, X.; Liu, J.-L.; Zhang, Z.; Na, B.; Shi, W.; Wang, B.-W.; Powell, A.K.; Chibotaru, L.F.; et al. Influence of Guest Exchange on the Magnetization Dynamics of Dilanthanide Single-Molecule-Magnet Nodes within a Metal-Organic Framework. *Angew. Chem.* **2015**, *54*, 9861–9865. [CrossRef]
17. Zhou, Q.; Yang, F.; Xin, B.; Zeng, G.; Zhou, X.; Liu, K.; Ma, D.; Li, G.; Shi, Z.; Feng, S. Reversible switching of slow magnetic relaxation in a classic lanthanide metal-organic framework system. *Chem. Commun.* **2013**, *49*, 8244–8246. [CrossRef]
18. Suzuki, K.; Sato, R.; Mizuno, N. Reversible switching of single-molecule magnet behaviors by transformation of dinuclear Dysprosium cores in polyoxometalates. *Chem. Sci.* **2013**, *4*, 596–600. [CrossRef]
19. Vallejo, J.; Pardo, E.; Viciano-Chumillas, M.; Castro, I.; Amoros, P.; Déniz, M.; Ruiz-Pérez, C.; Yuste-Vivas, C.; Krzystek, J.; Julve, M.; et al. Reversible solvatomagnetic switching in a single-ion magnet from an entatic state. *Chem. Sci.* **2017**, *8*, 3694–3702. [CrossRef]
20. Pinkowicz, D.; Ren, M.; Zheng, L.-M.; Sato, S.; Hasegawa, M.; Morimoto, M.; Irie, M.; Breedlove, B.K.; Cosquer, G.; Katoh, K.; et al. Control of the Single-Molecule Magnet Behavior of Lanthanide-Diarylethene Photochromic Assemblies by Irradiation with Light. *Chem. Eur. J.* **2014**, *20*, 12502–12513. [CrossRef]
21. Fetoh, A.; Cosquer, G.; Morimoto, M.; Irie, M.; El-Gammal, O.; El-Reash, G.A.; Breedlove, B.K.; Yamashita, M. Photo-activation of Single Molecule Behavior in a Manganese-based Complex. *Sci. Rep.* **2016**, *6*, 23785. [CrossRef]
22. Jiang, W.; Jiao, C.; Meng, Y.; Zhao, L.; Liu, Q.; Liu, T. Switching single chain magnet behavior via photoinduced bidirectional metal-to-metal charge transfer. *Chem. Sci.* **2018**, *9*, 617–622. [CrossRef] [PubMed]
23. Cosquer, G.; Kamila, M.; Li, Z.-Y.; Breedlove, B.K.; Yamashita, M. Photo-Modulation of Single-Molecule Magnetic Dynamics of a Dysprosium Dinuclear Complex via a Diarylethene Bridge. *Inorganics* **2018**, *6*, 9. [CrossRef]
24. Fetoh, A.; Cosquer, G.; Morimoto, M.; Irie, M.; El-Gammal, O.; El-Reash, G.M.A.; Breedlove, B.K.; Yamashita, M. Synthesis, Structures, and Magnetic Properties of Two Coordination Assemblies of Mn(III) Single Molecule Magnets Bridged via Photochromic Diarylethene Ligands. *Inorg. Chem.* **2019**, *58*, 2307–2314. [CrossRef] [PubMed]
25. Gonidec, M.; Davies, E.S.; McMaster, J.; Amabilino, D.B.; Veciana, J. Probing the Magnetic Properties of Three Interconvertible Redox States of a Single-Molecule Magnet with Magnetic Circular Dichroism Spectroscopy. *J. Am. Chem. Soc.* **2010**, *132*, 1756–1757. [CrossRef] [PubMed]
26. Norel, L.; Feng, M.; Bernot, K.; Roisnel, T.; Guizouarn, T.; Costuas, K.; Rigaut, S. Redox Modulation of Magnetic Slow Relaxation in a 4f-Based Single-Molecule Magnet with a 4d Carbon-Rich Ligand. *Inorg. Chem.* **2014**, *53*, 2361–2363. [CrossRef]
27. Dickie, C.M.; Laughlin, A.L.; Wofford, J.D.; Bhuvanesh, N.S.; Nippe, M. Transition metal redox switches for reversible "on/off" and "slow/fast" single-molecule magnet behavior in Dysprosium and erbium bis-diamidoferrocene complexes. *Chem. Sci.* **2017**, *8*, 8039–8049. [CrossRef]
28. Liu, J.-L.; Chen, Y.-C.; Zheng, Y.-Z.; Lin, W.-Q.; Ungur, L.; Wernsdorfer, W.; Chibotaru, L.F.; Tong, M.-L. Switching the anisotropy barrier of a single-ion magnet by symmetry change from quasi-D_{5h} to quasi-O_h. *Chem. Sci.* **2013**, *4*, 3310–3316. [CrossRef]
29. Da Cunha, T.T.; Jung, J.; Boulon, M.E.; Campo, G.; Pointillart, F.; Pereira, C.L.; Le Guennic, B.; Cador, O.; Bernot, K.; Pineider, F.; et al. Magnetic Poles Determinations and Robustness of Memory Effect upon Solubilization in a Dy^{III}-Based Single Ion Magnet. *J. Am. Chem. Soc.* **2013**, *135*, 16332–16335. [CrossRef]
30. Pointillart, F.; Le Guennic, B.; Golhen, S.; Cador, O.; Ouahab, L. Slow magnetic relaxation in radical cation tetrathiafulvalene-based lanthanide(III) dinuclear complexes. *Chem. Commun.* **2013**, *49*, 11632–11634. [CrossRef]
31. Pointillart, F.; Le Guennic, B.; Cador, O.; Maury, O.; Ouahab, L. Lanthanide Ion and Tetrathiafulvalene-Based Ligand as a "magic" Couple toward Luminescence, Single Molecule Magnets, and Magnetostructural Correlations. *Acc. Chem. Res.* **2015**, *48*, 2834–2842. [CrossRef]
32. Kuropatov, V.; Klementieva, S.; Fukin, G.; Mitin, A.; Ketlov, S.; Budnikova, Y.; Cherkasov, V.; Abakumov, G. Novel method for the synthesis of functionalized tetrathiafulvalenes, an acceptor–donor–acceptor molecule comprising of two o-quinone moieties linked by a TTF bridge. *Tetrahedron* **2010**, *66*, 7605–7611. [CrossRef]

33. Chalkov, N.O.; Cherkasov, V.K.; Abakumov, G.A.; Romanenko, G.V.; Ketkov, S.Y.; Smolyaninov, I.V.; Starikov, A.G.; Kuropatov, V.A. Compactly Fused o-Quinone-Extended Tetrathiafulvalene-o-Quinone Triad—A Redox-Amphoteric Ligand. *Eur. J. Org. Chem.* **2014**, *2014*, 4571–4576. [CrossRef]
34. Pointillart, F.; Klementieva, S.; Kuropatov, V.; Le Gal, Y.; Golhen, S.; Cador, O.; Cherkasov, V.; Ouahab, L. A single molecule magnet behavior in a D3h symmetry Dy^{III} complex involving a quinone-tetrathiafulvalene-quinone bridge. *Chem. Commun.* **2012**, *48*, 714–716. [CrossRef]
35. Flores Gonzalez, J.; Cador, O.; Ouahab, L.; Norkov, S.; Kuropatov, V.; Pointillart, F. Field-Induced Dysprosium Single-Molecule Magnet Involving a Fused o-Semiquinone-Extended-Tetrathiafulvalene-o-Semiquinone Bridging Triad. *Inorganics* **2018**, *6*, 45. [CrossRef]
36. Pointillart, F.; Flores Gonzalez, J.; Montigaud, V.; Tesi, L.; Cherkasov, V.; Le Guennic, B.; Cador, O.; Ouahab, L.; Sessoli, R.; Kuropatov, V. Redox- and Solvato-Magnetic Switching in a Tetrathiafulvalene-Based Triad Single-Molecule Magnet. *Inorg. Chem. Front.* **2020**, *7*, 2322–2334. [CrossRef]
37. Lefeuvre, B.; Flores Gonzalez, J.; Gendron, F.; Dorcet, V.; Riobé, F.; Cherkasov, V.; Maury, O.; Le Guennic, B.; Cador, O.; Kuropatov, V.; et al. Redox-Modulations of Photophysical and Single-Molecule Magnet Properties in Ytterbium Complexes Involving Extended-TTF Triads. *Molecules* **2020**, *25*, 492. [CrossRef]
38. Pointillart, F.; Jung, J.; Berraud-Pache, R.; Le Guennic, B.; Dorcet, V.; Golhen, S.; Cador, O.; Maury, O.; Guyot, Y.; Decurtins, S.; et al. Luminescence and Single-Molecule Magnet Behavior in LanthanideComplexes Involving a Tetrathiafulvalene-Fused Dipyridophenazine Ligand. *Inorg. Chem.* **2015**, *54*, 5384–5397. [CrossRef]
39. Fernandez-Garcia, G.; Flores Gonzalez, J.; Ou-Yang, J.-K.; Saleh, N.; Pointillart, F.; Cador, O.; Guizouarn, T.; Totti, F.; Ouahab, L.; Crassous, J.; et al. Slow Magnetic Relaxation in Chiral Helicene-Based Coordination Complex of Dysprosium. *Magnetochemistry* **2017**, *3*, 2. [CrossRef]
40. Galangau, O.; Flores Gonzalez, J.; Montigaud, V.; Dorcet, V.; Le Guennic, B.; Cador, O.; Pointillart, F. Dysprosium Single-Molecule Magnets Involving 1,10-Phenantroline-5,6-dione Ligand. *Magnetochemistry* **2020**, *6*, 19. [CrossRef]
41. Jones, A.E.; Christensen, C.A.; Perepichka, D.F.; Batsanov, A.S.; Beeby, A.; Low, P.J.; Bryce, M.R.; Parker, A.W. Photochemistry of the π-Extended 9,10-Bis(1,3-dithiol-2-ylidene)-9,10-dihydroanthracene System: Generation and Characterisation of the Radical Cation, Dication, and Derived Products. *Chem. Eur. J.* **2001**, *7*, 973–978. [CrossRef]
42. Cooper, W.F.; Edmonds, J.W.; Wudl, F.; Coppens, P. The 2-2′-bi-1,3-dithiole. *Cryst. Struct. Commun.* **1974**, *3*, 23–26.
43. Ellern, A.; Bernstein, J.; Becker, J.Y.; Zamir, S.; Shahal, L.; Cohen, S. A New Polymorphic Modification of tetrathiafulvalene. Crystal Structure, Lattice Energy and Intermolecular Interactions. *Chem. Mater.* **1994**, *6*, 1378–1385. [CrossRef]
44. Kahn, O. *Molecular Magnetism*; VCH: Weinhem, Germany, 1993.
45. Reta, D.; Chilton, N.F. Uncertainty estimates for magnetic relaxation times and magnetic relaxation parameters. *Phys. Chem. Chem. Phys.* **2019**, *21*, 23567–23575. [CrossRef] [PubMed]
46. Dekker, C.; Arts, A.F.M.; Wijn, H.W.; van Duyneveldt, A.J.; Mydosh, J.A. Activated dynamics in a two-dimensional Ising spin glass: $Rb_2Cu_{1-x}Co_xF_4$. *Phys. Rev. B* **1989**, *40*, 11243–11251. [CrossRef] [PubMed]
47. Cole, K.S.; Cole, R.H. Dipersion and Absorption in Dielectrics I. Alternating Current Characteristics. *J. Chem. Phys.* **1941**, *9*, 341–351. [CrossRef]
48. Abragam, A.; Bleaney, B. *Electron Paramagnetic Resonance of Transition Ions*; Clarendon Press: Oxford, UK, 1970.
49. Singh, A.; Shrivastava, K.N. Optical-acoustic two-phonon relaxation in spin systems. *Phys. Status Solidi B* **1979**, *95*, 273–277. [CrossRef]
50. Shirivastava, K.N. Theory of Spin-Lattice Relaxation. *Phys. Status Solidi B* **1983**, *177*, 437–458. [CrossRef]
51. Goodwin, C.A.P.; Reta, D.; Ortu, F.; Chilton, N.F.; Mills, D.P. Synthesis and Electronic Structures of Heavy Lanthanide Metallocenium Cations. *J. Am. Chem. Soc.* **2017**, *139*, 18714–18724. [CrossRef]
52. Evans, P.; Reta, D.; Whitehead, G.F.S.; Chilton, N.F.; Mills, D.P. Bis-Monophospholyl Dysprosium Cation Showing Magnetic Hysteresis at 48 K. *J. Am. Chem. Soc.* **2019**, *141*, 19935–19940. [CrossRef]
53. Pedersen, K.S.; Dreiser, J.; Weihe, H.; Sibille, R.; Johannesen, H.V.; Sorensen, M.A.; Nielsen, B.E.; Sigrist, M.; Mutka, H.; Rols, S.; et al. Design of Single-Molecule Magnets: Insufficiency of the Anisotropy Barrier as the Sole Criterion. *Inorg. Chem.* **2015**, *54*, 7600–7606. [CrossRef]

54. Zadrozny, J.M.; Atanasov, M.; Bryan, A.M.; Lin, C.-Y.; Rekken, B.D.; Power, P.P.; Neese, F.; Long, J.R. Slow magnetization dynamics in a series of two-coordinate iron(II) complexes. *Chem. Sci.* **2013**, *4*, 125–138. [CrossRef]
55. Chibotaru, L.F.; Ungur, L.; Soncini, A. The Origin of Nonmagnetic Kramers Doublets in the Ground State of Dysprosium Triangles: Evidence for a Toroidal Magnetic Moment. *Angew. Chem.* **2008**, *47*, 4126–4129. [CrossRef] [PubMed]
56. Lunghi, A.; Totti, F. The role of Anisotropic Exchange in Single Molecule Magnets: A CASSCF/NEVPT2 Study of the Fe4 SMM Building Block $[Fe_2(OCH_3)_2(dbm)_4]$ Dimer. *Inorganics* **2016**, *4*, 28. [CrossRef]
57. Vooshin, A.I.; Shavaleev, N.M.; Kazakov, V.P. Chemiluminescence of praseodymium (III), neodymium (III) and ytterbium (III) β-diketonates in solution excited from 1,2-dioxetane decomposition and singlet-singlet energy transfer from ketone to rare-earth β-diketonates. *J. Lumin.* **2000**, *91*, 49–58. [CrossRef]
58. Sheldrick, G.L. SHELXT—Integrated space-group and crystal-structure determination. *Acta Crystallogr. Sect. A Found. Adv.* **2015**, *71*, 3–8. [CrossRef] [PubMed]
59. Sheldrick, G.M. Crystal structure refinement with SHELXL. *Acta Crystallogr. Sect. C Struct. Chem.* **2015**, *71*, 3–8. [CrossRef] [PubMed]
60. Spek, A.L. Single-crystal structure validation with the program PLATON. *J. Appl. Crystallogr.* **2003**, *36*, 7–13. [CrossRef]
61. Aquilante, F.; Autschbach, J.; Carlson, R.K.; Chibotaru, L.F.; Delcey, M.G.; De Vico, L.; Galván, I.F.; Ferré, N.; Frutos, L.M.; Gagliardi, L.; et al. Molcas 8: New Capabilities for Multiconfigurational Quantum Chemical Calculations across the Periodic Table. *J. Comput. Chem.* **2016**, *37*, 506–541. [CrossRef]
62. Roos, B.O.; Taylor, P.R.; Siegbahn, P.E.M. A Complete Active Space SCF Method (CASSCF) Using a Density Matrix Formulated Super-CI Approach. *Chem. Phys.* **1980**, *48*, 157–173. [CrossRef]
63. Malmqvist, P.Å.; Roos, B.O.; Schimmelpfennig, B. The Restricted Active Space (RAS) State Interaction Approach with Spin-Orbit Coupling. *Chem. Phys. Lett.* **2002**, *357*, 230–240. [CrossRef]
64. Malmqvist, P.-Å.; Roos, B.O. The CASSCF State Interaction Method. *Chem. Phys. Lett.* **1989**, *155*, 189–194. [CrossRef]
65. Chibotaru, L.F.; Ungur, L. Ab Initio Calculation of Anisotropic Magnetic Properties of Complexes. I. Unique Definition of Pseudospin Hamiltonians and Their Derivation. *J. Chem. Phys.* **2012**, *137*, 064112. [CrossRef] [PubMed]
66. Aquilante, F.; Malmqvist, P.-Å.; Pedersen, T.B.; Ghosh, A.; Roos, B.O. Cholesky Decomposition-Based Multiconfiguration Second-Order Perturbation Theory (CD-CASPT2): Application to the Spin-State Energetics of Co^{III}(diiminato)(NPh). *J. Chem. Theory Comput.* **2008**, *4*, 694–702. [CrossRef] [PubMed]
67. Roos, B.O.; Lindh, R.; Malmqvist, P.A.; Veryazov, V.; Widmark, P.O. Main Group Atoms and Dimers Studied with A New Relativistic ANO Basis Set. *J. Phys. Chem. A* **2004**, *108*, 2851–2858. [CrossRef]
68. Roos, B.O.; Lindh, R.; Malmqvist, P.; Veryazov, V.; Widmark, P.O.; Borin, A.C. New Relativistic Atomic Natural Orbital Basis Sets for Lanthanide Atoms with Applications to the Ce Diatom and LuF_3. *J. Phys. Chem. A* **2008**, *112*, 11431–11435. [CrossRef] [PubMed]